Available online at www.sciencedirect.com
ScienceDirect
Comput. Methods Appl. Mech. Engrg. 197 (2008) 933–945
Computer methods in applied mechanics and engineering
www.elsevier.com/locate/cma

Flux reconstruction and solution post-processing in mimetic finite difference methods

Andrea Cangiani [a], Gianmarco Manzini [b,*]

[a] *Dipartimento di Matematica, Università di Pavia, via Ferrata 1, I-27100 Pavia, Italy*
[b] *Istituto di Matematica Applicata e Tecnologie Informatiche – CNR, via Ferrata 1, I-27100 Pavia, Italy*

Received 22 December 2006; received in revised form 27 July 2007; accepted 19 September 2007
Available online 7 October 2007

Abstract

We present a post-processing technique for the mimetic finite difference solution of diffusion problems in mixed form. Our post-processing method yields a piecewise linear approximation of the scalar variable that is second-order accurate in the L^2-norm on quite general polyhedral meshes, including non-convex and non-matching elements. The post-processing is based on the reconstruction of vector fields projected onto the mimetic space of vector variables. This technique is exact on constant vector fields and is shown to be independent of the mimetic scalar product choice if a local consistency condition is satisfied. The post-processing method is computationally inexpensive. Optimal performance is confirmed by numerical experiments.

Keywords: Polyhedral mesh; Mimetic finite difference method; Compatible discretization; Solution post-processing; Gradient reconstruction; Super-convergence

1. Introduction

The mimetic finite difference (MFD) method is a relatively new technique for the approximation of partial differential equations (PDEs) that stems from support-operator methods [25–27]. The method has been applied to steady elliptic problems with anisotropic and rough diffusion tensor [13,16,28], electromagnetic problems [15,19], flow simulations in porous media [14], and gas dynamics [12].

The basic idea behind the MFD techniques is to define difference operators that *mimic* the behavior of invariant differential operators like divergence, gradient, and curl [17–19]. The discrete operators are required to satisfy discrete analogs of the fundamental theorems of vector calculus that hold for their continuous counterparts. For instance, the discrete gradient is naturally defined as the adjoint of the discrete divergence with respect to the scalar products acting on the discrete scalar and vector fields [17]. The composition of the discrete divergence and gradient yields the discrete form of the Laplace's operator. This approach permits the design of schemes that embody conservation laws and solution symmetries.

The most recent mimetic methods [8,11,21–23] are formulated on general two- and three-dimensional meshes, including non-convex and non-matching polyhedra. An extension to meshes that include polyhedra with curved faces has also been proposed in Refs. [9,10]. Flexibility in mesh design is an obvious advantage when dealing with complex solution domains and heterogeneous materials. Moreover, allowing non-matching and non-convex elements simplifies adaptive mesh refinement, particularly in the coarsening phase, making it a completely local process.

Another feature of the mimetic discretization proposed in [8] is the connection with the lowest order Raviart–Thomas finite element method on quadrilateral [3] and triangular grids [24]. The MFD methods have also obvious similarities with *finite volumes* and *compatible finite element* discretizations [2]. Coherently, the MFD formulation of

* Corresponding author. Tel.: +39 0382 548 238; fax: +39 0382 548 300.
E-mail addresses: andrea.cangiani@unipv.it (A. Cangiani), marco.manzini@imati.cnr.it (G. Manzini).

0045-7825/$ - see front matter © 2007 Elsevier B.V. All rights reserved.
doi:10.1016/j.cma.2007.09.019

Refs. [8,11] replicates the dual mixed formulation for the *scalar solution* and *vector flux* fields by means of discrete scalar and vector fields and a discrete version of the Gauss–Green (integration-by-part) formula. The discrete scalar solution consists of a set of cell-based unknowns providing a piecewise constant approximation of the continuous solution. The discrete vector variable consists of a set of face-based unknowns approximating the normal components of the continuous flux field on mesh faces. Based on this setting, a family of inexpensive mimetic schemes is designed whose members differ in the definition of the scalar product acting on vectors [11]. The piecewise constant approximation of the scalar solution is first-order accurate in the L^2-norm, while the solution degrees-of-freedom quadratically converge to the solution cell averages due to a super-convergence effect.

In this context, we propose a post-processing procedure which exploits the super-convergence property just mentioned to provide a more accurate numerical approximation of the solution. The post-processing is based on a local reconstruction of vector fields from their normal face averages. The reconstruction algorithm is designed to yield the best piecewise constant approximation of a generic non-constant vector field with respect to the norm induced by the mimetic scalar product.

The numerical solution is post-processed as follows. First, we obtain a piecewise constant approximation of the solution gradient by applying the reconstruction procedure to the mimetic vector flux. Second, we define a piecewise linear approximation of the scalar solution by using the piecewise constant mimetic solution and the reconstructed gradient. We remark that the local reconstruction of cell gradients is a well-established technique in cell-centered finite volume methods [5–7], although, in such context, the input data are the approximate cell averages.

We prove that the piecewise linear solution quadratically converges to the exact solution in the L^2-norm. This result is obtained under the very general mesh regularity assumptions used in [8] to prove super-convergence in the discrete MFD norm. The optimal performance of the reconstruction is confirmed by numerical experiments on meshes formed by convex or L-shaped (i.e. non-convex and non-matching) elements.

The paper is organized as follows. In Section 2 we introduce the necessary assumptions on the partition and we formulate the Mimetic Finite Difference method. In Section 3 we characterize the vector fields reconstruction procedure. The post-processing of the solution is analyzed in Section 4. Finally, Section 5 is dedicated to the numerical tests confirming the validity of the theoretical analysis and Section 6 to some conclusions.

2. Formulation of the MFD method

Let $\Omega \subset \mathbb{R}^d$ be a bounded, convex, and open polyhedron for $d=3$ or polygon for $d=2$ with Lipschitz continuous boundary. We consider the boundary value problem

$$\begin{aligned} \mathbf{F} &= \mathsf{K}\nabla p && \text{in} \quad \Omega, \\ -\operatorname{div}\mathbf{F} &= b && \text{in} \quad \Omega, \\ p &= g^D && \text{on} \quad \Gamma, \end{aligned} \tag{1}$$

for the *flux* $\mathbf{F}$ and the *scalar solution* p. In (1) $b \in H^1(\Omega)$ and $g^D \in H^{1/2}(\Omega)$ are, respectively, the source function and the boundary data, and K is a full symmetric tensor describing the material properties. We assume that K is constant inside each partition element and that it is *strongly elliptic*, i.e. that there exist two constants κ_* and κ^* such that

$$\kappa_*\|\mathbf{v}\|^2 \leqslant \|\mathsf{K}^{1/2}\mathbf{v}\|^2 \leqslant \kappa^*\|\mathbf{v}\|^2 \quad \forall \mathbf{v} \in \mathbb{R}^d. \tag{2}$$

Under these assumptions the boundary value problem (1) is well-posed and admits a unique solution in $H^2(\Omega)$. It is worth noting that the weaker regularity assumption $b \in L^2$ would still provide a solution in $H^2(\Omega)$. Nonetheless, the theoretical result that is proved in this paper requires that $b \in H^1(\Omega)$.

2.1. Mesh regularity assumptions

Let $\mathscr{T}_h$ be a non-overlapping conformal partition of Ω into polyhedral elements (polygons in 2D). For every element E we denote its d-dimensional Lebesgue measure by $|E|$ and its diameter by h_E. Similarly, $|e|$ denotes the $(d-1)$-measure of the face e and $|l|$ denotes the $(d-2)$ measure of the edge l. The notation ∂E may denote the boundary of the element E or the union of the element faces. We also set, as usual, $h = \sup_E h_E$.

Since this work is based on the *a priori* analysis of Ref. [8] and the family of methods developed in Ref. [11], we consider the same set of assumptions detailed there. We report these assumptions below for the sake of the reader's convenience and for future reference in the paper. The assumptions are formulated for the case $d=3$; the restriction to the case $d=2$ is straightforward.

- (M1) There exist two positive integers N_E and N_e such that every element E has a number of faces k_E that is bounded by N_E and every face e has a number of edges k_e that is bounded by N_e.
- (M2) There exist three positive constants v^*, a^*, l^* (for volume, area and length, respectively) such that for every element E there holds $v^* h_E^3 \leqslant |E|$, $a^* h_E^2 \leqslant |e|$, $l^* h_E \leqslant |l|$ for all faces e and edges l of E.
- (M3) There exists a positive number τ^* such that each element E is star-shaped with respect to all points of a ball of radius $\tau^* h_E$ and center at a point $C_E \in E$.
- (M4) There exists a positive number γ^* such that each face $e \in \partial E$ is star-shaped with respect to all points of a ball of radius $\gamma^* h_E$ and center at a point $C_e \in e$.
- (M5) For every element E and for every face $e \in \partial E$ there exists a pyramid contained in E and having base coincident with e, height equal to $\gamma^* h_E$, and such that the projection of its vertex onto e is C_e.

We shall make direct use of Assumptions (M2) (shape-regularity) and (M3) (star-shaped elements). In particular,

condition (M2) implies that $|E| \approx h_E^d$ and $|e| \approx h_E^{(d-1)}$, where the symbol "$\approx$" indicates that the left-hand sides are uniformly bounded from above and from below by the right-hand sides.

2.2. Four steps towards mimetic finite differences

Following [8], we formulate the mimetic finite difference method in four steps.

The first step consists in specifying the two linear spaces, respectively denoted by Q_h and X_h, of the degrees-of-freedom of discrete scalar fields and fluxes.

We associate the degrees-of-freedom of scalar fields to mesh cells so that

$$\text{if } \mathbf{q} \in Q_h \quad \text{then } \mathbf{q} = \{\mathbf{q}_E\}_{E\in\mathscr{T}_h} \quad \text{with } \mathbf{q}_E \in \mathbb{R}.$$

We associate the degrees-of-freedom of fluxes to mesh faces so that

$$\text{if } \mathbf{G} \in X_h \quad \text{then } \mathbf{G} = \{\mathbf{G}_E^e\}_{E\in\mathscr{T}_h}^{e\in\partial E} \quad \text{with } \mathbf{G}_E^e \in \mathbb{R},$$

with the additional assumption that

$$G_{E_1}^e + G_{E_2}^e = 0 \quad \text{when } e \in E_1 \cap E_2, \quad E_1, E_2 \in \mathscr{T}_h,$$

to impose the continuity of the normal component of the flux. In view of the previous definitions, the dimension of Q_h equals the number of mesh cells and the dimension of X_h equals the number of mesh faces. We also introduce two projection operators for, respectively, $\mathbf{q} \in L^1(\Omega)$ and $\mathbf{G} \in (L^s(\Omega))^d$ with $s > 2$ and $\operatorname{div}\mathbf{G} \in L^2(\Omega)$ as

$$(q^I)_E = \frac{1}{|E|}\int_E q\,\mathrm{d}V \quad \text{for all } E \in \mathscr{T}_h,$$

$$(\mathbf{G}^I)_E^e = \frac{1}{|e|}\int_e \mathbf{n}_E^e \cdot \mathbf{G}\,\mathrm{d}S \quad \text{for all } e \in \partial E, E \in \mathscr{T}_h,$$

and denote the restriction of $\mathbf{G}^I \in X_h$ to the faces in ∂E by $\mathbf{G}_E = \{(\mathbf{G}^I)_E^e\}^{e\in\partial E}$.

In the second step, we equip Q_h and X_h with two suitable *scalar products*. We define the scalar product in Q_h as

$$[\mathbf{p},\mathbf{q}]_{Q_h} = \sum_{E\in\mathscr{T}_h} |E| p_E q_E, \tag{3}$$

which corresponds to the L^2-scalar product for piecewise constant functions. To define a scalar product in X_h, we first introduce a local scalar product acting on the restriction of X_h to E:

$$[\mathbf{F},\mathbf{G}]_E = \sum_{s,t=1}^{k_E} M_E^{s,t} F_E^{e_s} G_E^{e_t}. \tag{4}$$

We shall eventually assign the elemental scalar product by specifying the entries of the $k_E \times k_E$-sized matrix $\mathsf{M}_E = \{M_E^{s,t}\}$, which is consequently required to be symmetric and positive definite. The details concerning the construction of M_E are given in the following sub-section. We complete the definition of the scalar product in X_h by assembling the element-wise contribution from each element E:

$$[\mathbf{F},\mathbf{G}]_{X_h} = \sum_{E\in\mathscr{T}_h} [\mathbf{F},\mathbf{G}]_E. \tag{5}$$

In the following, the symbols $|||\cdot|||_{Q_h}$, $|||\cdot|||_E$, and $|||\cdot|||_{X_h}$ will indicate the norms induced by the scalar products (3)–(5).

In the third step, we define the *discrete divergence operator* $\operatorname{div}_h : X_h \to Q_h$ as

$$(\operatorname{div}_h\mathbf{G})_E = \frac{1}{|E|}\sum_{s=1}^{k_E} |e_s| \mathbf{G}_E^{e_s}, \quad \text{for } \mathbf{G} \in X_h.$$

The definition above is consistent with the Gauss divergence theorem.

In the fourth step, we define the *discrete flux operator* $\mathscr{G}_h : Q_h \to X_h$ as the adjoint of the discrete divergence operator with respect to the scalar products of Q_h and X_h. Thus,

$$[\mathbf{G}, \mathscr{G}_h\mathbf{q}]_{X_h} = -[\operatorname{div}_h\mathbf{G}, \mathbf{q}]_{Q_h} \tag{6}$$

for all $\mathbf{q} \in Q_h$ and $\mathbf{G} \in X_h$. Formula (6) naturally establishes a discrete Green-like formula with respect to the scalar products of Q_h and X_h; in this sense, the operators div_h and $\mathscr{G}_h$ *mimic* the continuous ones.

The MFD method that we consider in this work relies on the following dual mixed formulation:

Find $(\mathbf{p}_h, \mathbf{F}_h) \in Q_h \times X_h$ *such that*:

$$[\mathbf{F}_h,\mathbf{G}]_{X_h} + [\mathbf{p}_h, \operatorname{div}_h\mathbf{G}]_{Q_h} = \langle \mathbf{g}, \mathbf{G}\rangle_{\partial\mathscr{T}_h} \quad \text{for all } \mathbf{G} \in X_h, \tag{7a}$$

$$[\operatorname{div}_h\mathbf{F}_h, \mathbf{q}]_{Q_h} = -[\mathbf{b},\mathbf{q}]_{Q_h} \quad \text{for all } \mathbf{q} \in Q_h, \tag{7b}$$

where $\mathbf{b} = b^I$ and

$$\langle \mathbf{g}, \mathbf{G}\rangle_{\partial\mathscr{T}_h} = \sum_{e\in\partial\mathscr{T}_h} |e| (\mathbf{g})^e (\mathbf{G})^e$$

and $(\mathbf{g})^e$ is the average of the Dirichlet boundary datum g^{D} on the face $e \in \partial\mathscr{T}_h$.

2.3. Construction of the scalar product of X_h

In this section, we describe the construction of the family of scalar products for X_h proposed in Ref. [11]. The construction is based on the assumption that the scalar product in X_h satisfies the following two conditions:

- *Stability:* there exist two constants C_*, $C^* > 0$ independent of h such that

$$C_* \sum_{s=1}^{k_E} |E| (G_E^{e_s})^2 \leqslant [\mathbf{G},\mathbf{G}]_E \leqslant C^* \sum_{s=1}^{k_E} |E| (\mathbf{G}_E^{e_s})^2 \tag{8}$$

  for all $\mathbf{G} \in X_h$ and for every element E;
- *Local consistency:* for every linear function $\mathbf{q}^1$ on $E \in \mathscr{T}_h$

$$[(\mathsf{K}_E \nabla q^1)^I, G]_E + \int_E q^1 \operatorname{div}_h G\,\mathrm{d}V = \sum_{s=1}^{k_E} G_E^{e_s} \int_{e_s} q^1\,\mathrm{d}S \tag{9}$$

  for all $\mathbf{G} \in X_h$.

Let $\hat{x}^{(i)}$ be the ith unit vector of the spatial coordinate system, X_E the position of the barycenter of the element E, and X_{e_s} the position of the barycenter of the sth face e_s of ∂E. Testing (9) with $q^1 = 1$ yields the definition of the discrete divergence operator, while testing with $q^1 = (x - x_E)_i = \hat{x}^{(i)} \cdot (x - x_E)$ for $i = 1, \ldots, d$ yields the conditions:

$$[(\mathsf{K}_E \hat{x}^{(i)})^I, G]_E = \sum_{s=1}^{k_E} G_E^{e_s} \int_{e_s} \hat{x}^{(i)} \cdot (x - x_E) \mathrm{d}S. \tag{10}$$

Notice that the right-hand side of (10) does not depend on the matrix M_E: it follows that all scalar products satisfying the consistency assumption give the same result if one of the factors is the interpolation of a constant vector field. Notice also that the scalar product is exact on the interpolation of constant vectors as, for any $i,j = 1, \ldots, d$, we have:

$$\begin{aligned}[(\mathsf{K}_E \hat{x}^{(i)})^I, (\mathsf{K}_E \hat{x}^{(j)})^I]_E &= \int_{\partial E} \hat{x}^{(i)} \cdot (x - x_E)(\mathsf{K}_E \hat{x}^{(j)}) \cdot n_E \, \mathrm{d}S \\ &= \int_E \hat{x}^{(i)} \cdot \mathsf{K}_E \hat{x}^{(j)} \, \mathrm{d}V = |E| (\mathsf{K}_E)_{i,j}. \end{aligned} \tag{11}$$

We reformulate conditions (10) in matrix form by introducing two $k_E \times d$ matrices N and R as follows. We rewrite (10) as

$$(\mathsf{K}_E \hat{x}^{(i)})^{I,t} \mathsf{M}_E G_E = \sum_{s=1}^{k_E} |e_s| (x_{e_s} - x_E)_i G_E^{e_s}. \tag{12}$$

Further, we define the matrix N in column- and row-partitioned form as

$$\mathsf{N} = \left[(\mathsf{K}_E \hat{x}^{(1)})^I \ldots (\mathsf{K}_E \hat{x}^{(d)})^I \right] = \begin{bmatrix} n_E^{e_1,t} \\ \vdots \\ n_E^{e_{k_E},t} \end{bmatrix} \mathsf{K}_E \, .$$

The equivalence between the two formulations above easily follows by using the interpolation operator. Finally we define the matrix R in row-partitioned form as

$$\mathsf{R} = \begin{bmatrix} |e_1| (x_{e_1} - x_E)^t \\ \vdots \\ |e_{k_E}| (x_{e_{k_E}} - x_E)^t \end{bmatrix}.$$

We can now rewrite the local consistency condition (12) in terms of the matrices N and R as

$$\mathsf{M}_E \mathsf{N} = \mathsf{R}. \tag{13}$$

A direct calculation based on Gauss–Green formula also shows that (*cf.* [11]):

$$\mathsf{R}^t \mathsf{N} = |E| \mathsf{K}_E.$$

Imposing local consistency (13) and symmetry, we obtain an under-determined linear system for the components of M_E. The general solution of such linear system is given by

$$\mathsf{M}_E = \mathsf{M}_E^0 + \delta \mathsf{M}_E,$$

where M_E^0 and $\delta \mathsf{M}_E$ are symmetric matrices satisfying, respectively, $\mathsf{M}_E^0 \mathsf{N} = \mathsf{R}$ and $\delta \mathsf{M}_E \mathsf{N} = 0$. As pointed out in [11], a choice that guarantees that M_E is positive definite and ensures the stability condition (8) is given by

$$\mathsf{M}_E^0 = \frac{1}{|E|} \mathsf{R} \mathsf{K}_E^{-1} \mathsf{R}^t \quad \text{and} \quad \delta \mathsf{M}_E = \mathsf{C} \mathsf{U} \mathsf{C}^t,$$

where the matrix U is symmetric and positive definite and the columns of C form a basis of the kernel of N, i.e. $\mathsf{N}^t \mathsf{C} = 0$. The above construction produces a family of suitable matrices M_E in function of U and, correspondingly, a family of scalar products for the vector space X_h. A possible choice for the matrix U is given by

$$\mathsf{U} = u|E| \mathrm{Trace}(\mathsf{K}_E^{-1}) \mathsf{I}_d, \tag{14}$$

where a convenient value for u is unity (*cf.* [11]). Moreover, for some suitable choice of U and the correction term $\delta \mathsf{M}_E$, several 'classical' schemes may be retrieved as shown by the following examples.

Example 1. When the mesh $\mathscr{T}_h$ is formed by simplexes, e.g. triangles if $d = 2$ and tetrahedrons if $d = 3$, then U becomes a 1×1 matrix, thus providing a one-parameter family as observed in [24]. A straightforward calculation shows that the choice

$$\mathsf{U} = \left[\frac{\sum_{i=1}^{k_E} (x_{e_i} - x_E)^t \mathsf{K}_E^{-1} (x_{e_i} - x_E)}{d^2 (d+1) |E|} \right] \quad \text{and} \quad \mathsf{C} = \begin{bmatrix} |e_1| \\ \vdots \\ |e_d| \end{bmatrix}$$

yields the local scalar product matrix of the RT_0 finite element space.

Example 2. Assume that the mesh $\mathscr{T}_h$ is formed by d-dimensional cuboids. Then, the MFD discretisation of the Laplace operator yields, with the choice $U = \mathsf{I}_d$, the classical central finite difference scheme for the scalar variable unknowns.

The proof of the super-convergence property of the MFD method relevant to our post-processing technique is based on the hypothesis that the local scalar product is linked to a lifting operator.

Definition 1. Set $X_E = X_h|_E$. We say that a linear map $\mathscr{L}_E(G_E) : X_E \to L^2(E)$ is a P^0-compatible lifting in $E \in \mathscr{T}_h$ if, for all $\mathbf{G}_E \in X_E$, it holds

$$\begin{aligned} &\mathscr{L}_E(G_E)|_{\partial E} = G_E \quad \text{on } \partial E, \\ &\mathrm{div} \mathscr{L}_E(G_E) = (\mathrm{div}_h G)|_E \quad \text{in } E \end{aligned}$$

and, for all constant vector-valued functions $\mathbf{c}$, it holds

$$\mathscr{L}_E(c_E^I) = c.$$

It is easy to check that if $\mathscr{L}_E(F_E)$ is a P^0-compatible lifting, then the choice

$$[F, G]_E = \int_E \mathsf{K}_E^{-1} \mathscr{L}_E(F_E) \cdot \mathscr{L}_E(G_E) \mathrm{d}V \tag{15}$$

defines a scalar product in X_E that satisfies the consistency conditions (10). From (10) it follows that, if one of the factors is the interpolation of a constant vector field, then the value of (15) is independent of the lifting operator. In [10], it is shown that a large sub-class of the set of matrices M_E satisfying the consistency condition defines scalar products given by P^0-compatible liftings. We shall verify experimentally that super-convergence is attained for a wide class of scalar products, suggesting that the need of the lifting operator is only theoretical.

3. Reconstruction of vector fields

Given a vector field $v(x) \in \mathbb{R}^d$, let $\mathbf{v}^I \in X_h$ be its interpolation, and $v_E^I \in \mathbb{R}^{k_E}$ the restriction of $\mathbf{v}^I$ to the faces of ∂E.

Definition 2. We define the vector field v_E^R, reconstruction of $\mathbf{v}(\mathbf{x})$ on E from v_E^I, by

$$v_{E,i}^R = \frac{1}{|E|}[(\mathsf{K}_E\hat{x}^{(i)})^I, v^I]_E \quad \text{for } i = 1,\dots,d. \tag{16}$$

A global piecewise constant reconstruction $v^R \in (\mathrm{P}^0(\mathscr{T}_h))^d$ of $\mathbf{v}(\mathbf{x})$ is given by setting $v^R|_E = v_E^R$ for all $E \in \mathscr{T}_h$.

As one of the two factors in (16) is the interpolation of a constant vector, the reconstructed field is the same for all scalar products satisfying local consistency. This fact is evidenced by the vector notation

$$v_E^R = \frac{1}{|E|}\mathsf{N}^t\mathsf{M}_E v_E^I = \frac{1}{|E|}\mathsf{R}^t v_E^I, \tag{17}$$

where we have used (13). In particular, when the scalar product is given by (15), the reconstruction is independent of the definition of the lifting operator $\mathscr{L}_E(\cdot)$.

Moreover, the reconstruction is exact for constant vector fields. Indeed, if $\mathbf{v}$ is constant, then for $i = 1,\dots,d$, we have:

$$v_{E,i}^R = \frac{1}{|E|}[(\mathsf{K}_E\hat{x}^{(i)})^I, v^I]_E = \frac{1}{|E|}\int_E \mathsf{K}_E^{-1}\mathsf{K}_E\hat{x}^{(i)}\cdot v\,\mathrm{d}V = \hat{x}^{(i)}\cdot v.$$

We characterize the reconstruction process in the following equivalent way.

Proposition 1. *The reconstructed vector field v_E^R is the best constant approximation of $\mathbf{v}(\mathbf{x})$ on E with respect to the local norm $|||\cdot|||_E$ induced by $[\cdot,\cdot]_E$. Formally,*

$$v_E^R = \operatorname*{argmin}_{w\in(\mathrm{P}^0(\Omega))^d} \frac{1}{2}|||w^I - v^I|||_E^2.$$

Proof. Let us consider the quadratic functional $\mathscr{J}_E(w) = \frac{1}{2}|||w^I - v^I|||_E^2$ defined for $\mathbf{w} \in (\mathrm{P}^0(\Omega))^d$. Its minimizer $\tilde{w} = \sum_{i=1}^d \tilde{w}_i\hat{x}^{(i)}$ must satisfy the null gradient condition $\nabla_w\mathscr{J}_E(\tilde{w}) = 0$, from which it follows that

$$[w^I, \tilde{w}^I - v^I]_E = 0 \Rightarrow [\tilde{w}^I, \tilde{w}^I]_E = [\tilde{w}^I, v^I]_E.$$

From the exactness of $[\cdot,\cdot]_E$ on constant vectors, we have that

$$[\tilde{w}^I, \tilde{w}^I]_E = \int_E \mathsf{K}_E^{-1}\tilde{w}\cdot\tilde{w}\,\mathrm{d}V = |E|\sum_{i=1}^d (\mathsf{K}_E^{-1}\tilde{w})_i\tilde{w}_i, \tag{18}$$

while, by using the definition of $\tilde{w}$, we obtain

$$\begin{aligned}[\tilde{w}^I, v^I]_E &= \left[\left(\sum_{i=1}^d \tilde{w}_i\hat{x}^{(i)}\right)^I, v^I\right]_E \\ &= \sum_{i=1}^d (\mathsf{K}_E^{-1}\tilde{w})_i[(\mathsf{K}_E\hat{x}^{(i)})^I, v^I]_E.\end{aligned} \tag{19}$$

The proposition statement follows by comparing (18) and (19). □

We shall now prove a further property of the reconstruction procedure, which only holds on a special set of polyhedra. Such a property is not used by any result proven subsequently in the paper. We say that a polyhedra is *semiregular* if

- it has an even number of faces;
- its faces can be grouped into parallel and congruent pairs;
- the midpoint of the segment connecting the barycenter of the faces of each pair coincides with the barycenter of the element.

For example, parallelograms and regular polygons with an even number of edges are semiregular.

Proposition 2. *Let E be a semiregular polyhedron and $\mathbf{v}(\mathbf{x})$ a linear vector field on E, i.e. $\mathbf{v}(\mathbf{x}) \in (P^1(E))^d$; then $v_E^R = v(x_E)$.*

Proof. Let e and e' denote two parallel and congruent faces. Consequently, $|e| = |e'|$, $n_E^e = -n_E^{e'}$ and $(x_e - x_E) = -(X_{e'} - x_E)$. This proposition follows by suitably re-writing formula (17). Indeed,

$$\begin{aligned}v_{E,i}^R &= \frac{1}{|E|}(\mathsf{R}^t v_E^I)_i = \frac{1}{2|E|}\sum_{e\in\partial E}[\mathsf{R}_{ei}(v_E^I)_E^e + \mathsf{R}_{e'i}(v_E^I)_E^{e'}] \\ &= \frac{1}{2|E|}\sum_{e\in\partial E}[|e|(x_e - x_E)_i\, n_E^e\cdot v(X_e) \\ &\quad + |e'|(x_{e'} - x_E)_i\, n_E^{e'}\cdot v(x_{e'})] \\ &= \frac{1}{|E|}\sum_{e\in\partial E}|e|(x_e - x_E)_i\, n_E^e\cdot\frac{v(X_e) + v(x_{e'})}{2}.\end{aligned}$$

As the field $\mathbf{v}(\mathbf{x})$ is linear in $\mathbf{x}$ and $x_E = (x_e + x_{e'})/2$, we finally have

$$\begin{aligned}v_{E,i}^R &= \frac{1}{|E|}\sum_{e\in\partial E}|e|(x_e - x_E)_i\, n_E^e\cdot v\left(\frac{x_e + x_{e'}}{2}\right) \\ &= \frac{1}{|E|}\int_{\partial E}(x - x_E)_i\, n_E^e\,\mathrm{d}S\cdot v(x_E) \\ &= \frac{1}{|E|}\int_E \nabla(\hat{x}^{(i)}\cdot(x - x_E))\,\mathrm{d}V\cdot v(x_E) = \hat{x}^{(i)}\cdot v(x_E).\end{aligned}$$

□

A similar super-closeness property was proven for parallelograms in [20].

In view of Definition (2), it is quite natural to formulate a reconstruction process for all vectors of X_h, without caring if they actually are interpolations of spatial vector fields. Given $\mathbf{F} \in X_h$ we reconstruct a constant field on E by setting

$$F^R_{E,i} = \frac{1}{|E|}[(\mathsf{K}_E \hat{x}^{(i)})^I, F]_E \quad \text{for } i = 1, \ldots, d.$$

The following proposition establishes the continuity of this element-wise reconstruction process.

Proposition 3. *Let K_E be the constant diffusion tensor field on $E \in \mathscr{T}_h$. Then, we have*

$$\|F^R_E\|_{L^2(E)} \leqslant \mathrm{Trace}(\mathsf{K}_E)^{1/2} |||F|||_E \quad \textit{for all } F \in X_h.$$

Proof. Definition 2, the Cauchy–Schwarz inequality and (11) yield

$$\begin{aligned}\|F^R_E\|^2_{L^2(E)} &= |E| \sum_{i=1}^d |F^R_{E,i}|^2 = \frac{1}{|E|} \sum_{i=1}^d [(\mathsf{K}_E \hat{x}^{(i)})^I, F]^2_E \\ &\leqslant \frac{1}{|E|} \sum_{i=1}^d |||(\mathsf{K}_E \hat{x}^{(i)})^I|||^2_E |||F|||^2_E \\ &= \mathrm{Trace}(\mathsf{K}_E) |||F|||^2_E,\end{aligned}$$

for any $\mathbf{F} \in X_h$. □

4. Post-processing of MFD solution

From the approximate MFD flux $\mathbf{F}_h \in X_h$ we construct the constant elemental flux

$$(F^R_{h,E})_i = \frac{1}{|E|}[(\mathsf{K}_E \hat{x}^{(i)})^I, F_h]_E.$$

In turn, this is used to derive the elemental solution gradient, denoted by the symbol "$\nabla_E p_h$", and defined by

$$\nabla_E p_h = \mathsf{K}_E^{-1} F^R_{h,E}.$$

Definition 3. The piecewise linear approximation of the scalar solution field $p^R_h \in \mathrm{P}^1(\mathscr{T}_h)$ is given on each $E \in \mathscr{T}_h$ by

$$p^R_h|_E := p^R_E(x) = p_{h,E} + \nabla_E p_h \cdot (x - x_E) \quad \text{for } x \in E.$$

Let us recall the following standard estimate. For a star-shaped subset E of $\mathbb{R}^d$ it holds

$$\|u - \bar{u}\|_{L^2(E)} \leqslant C h_E |u|_{H^1(E)} \quad \text{for all } u \in H^1(E), \tag{20}$$

where $\bar{u}$ denotes the L^2-projection of u on the space of constant functions on E. The following lemma extends (20) to linear polynomials as proven in the Appendix by averaging the error of the Taylor's expansion.

Lemma 1 (Averaged Taylor's polynomial). *Let $\mathscr{T}_h$ be a partition of Ω satisfying Assumptions* (M1)–(M5)*. Then, for every $p \in H^2(\Omega)$ it holds*

$$\sum_{E \in \mathscr{T}_h} \int_E \left| u(x) - \frac{1}{|E|} \int_E (u(y) + \nabla u(y) \cdot (x - y)) \mathrm{d}y \right|^2 \mathrm{d}x \leqslant C h^4 |u|_{H^2(\Omega)}. \tag{21}$$

Finally, we will use Agmon's inequality

$$\|u - \bar{u}\|^2_{L^2(e)} \leqslant C \left(\frac{1}{h_E} \|u - \bar{u}\|^2_{L^2(E)} + h_E |u - \bar{u}|^2_{H^1(E)} \right), \tag{22}$$

which holds for $u \in H^1(E)$ on every face $e \in \partial E$.

Let us recall the convergence results from the analysis of [8].

Lemma 2 (A priori estimates). *Let $(p, \mathbf{F})$ be the solution of problem (1) under the assumption (2), $p \in H^2(\Omega)$, and $(\mathbf{p}_h, \mathbf{F}_h)$ the MFD solution given by (7a) and (7b), under the mesh regularity assumptions* (M1)–(M5)*. Let, moreover, $\mathbf{p}^I$, $\mathbf{F}^I$ be the interpolations of p and $\mathbf{F}$, respectively. Then, we have*

$$|||F^I - F_h|||_{X_h} \leqslant C h \|p\|_{H^2(\Omega)}. \tag{23}$$

Assuming, moreover, that Ω is convex, we have

$$|||p^I - p_h|||_{Q_h} \leqslant C h [\|p\|_{H^2(\Omega)} + \|b\|_{H^1(\Omega)}]. \tag{24}$$

A super-convergence result for the approximation of the scalar solution is also needed. This result is proved by assuming that the local scalar product acting on $X_h|_e$ is associated with a suitable lifting operator [8]:

(L) for each element E the scalar product $[\cdot,\cdot]_E$ is defined by (15) through a P^0-compatible lifting operator $\mathscr{L}_E(\cdot)$ such that

$$\|\mathscr{L}_E(G^I) - G\|_{L^2(E)} \leqslant C h [E] \|G\|_{(H^1(E))^d} \quad \text{for all } G \in (H^1(E))^d.$$

Lemma 3 (Solution superconvergence). *Under the assumptions of Lemma 2 and the assumption* (L) *reported above for the lifting operator $\mathscr{L}_E(\cdot)$ we have*

$$|||p^I - p_h|||_{Q_h} \leqslant C h^2 [\|p\|_{H^2(\Omega)} + \|b\|_{H^1(\Omega)}]. \tag{25}$$

Our first result concerns the MFD solution error in the L^2-norm and is an easy consequence of 2 and of the averaged Taylor estimate (24).

Proposition 4. *Let p_h be the piecewise constant approximation of p corresponding to the degrees-of-freedom of $\mathbf{p}_h$. Under the assumptions of Lemma 2 we have*

$$\|p - p_h\|_{L^2(\Omega)} \leqslant C h [\|p\|_{H^2(\Omega)} + \|b\|_{H^1(\Omega)}].$$

Proof. Note that

$$\begin{aligned}\|p-p_h\|^2_{L^2(\Omega)} &= \sum_{E\in\mathscr{T}_h}\int_E |p(x)-p_{h,E}|^2\,\mathrm{d}V\\ &\leqslant \sum_{E\in\mathscr{T}_h}\left[\int_E |p(x)-\bar{p}|^2\,\mathrm{d}V+\int_E|\bar{p}-p_{h,E}|^2\,\mathrm{d}V\right]\\ &\leqslant C\sum_{E\in\mathscr{T}_h}h_E^2|p|^2_{H^1(E)}+\sum_{E\in\mathscr{T}_h}|E|(p^I)_E-p_{h,E}|^2\\ &\leqslant Ch^2|p|^2_{H^1(\Omega)}+|||p^I-p_h|||^2_{Q_h},\end{aligned}$$

where we used (20) and recognized the definition of the norm $|||\cdot|||_{Q_h}$. The estimate follows by using (24). □

We now prove that our post-processing technique guarantees an higher-order approximation of the scalar solution field. Let us start with the following Lemma.

Lemma 4. *Let E be a star-shaped subset of $\mathbb{R}^d$ satisfying Assumptions* (M1)–(M5)*. Then, if $p\in H^2(E)$ we have*

$$\|\overline{\nabla p}-\nabla_E p_h\|_{L^2(E)}\leqslant C'h_E|p|_{H^2(E)}+C''|||F^I-F_h|||_E,$$

where the real positive constants C' and C'' are independent of p and h_E.

Proof. Note that $\mathsf{K}_E\overline{\nabla p}=\overline{F}$ and $\overline{F}=(\overline{F}^I)^R$ since $\overline{F}$ is a constant vector field on E. Substituting $\mathsf{K}_E\nabla_E p_h=F^R_{h,E}$, using Proposition 3, adding and subtracting $\mathbf{F}^I$ and using the triangular inequality yield

$$\begin{aligned}\|\overline{\nabla p}-\nabla_E p_h\|_{L^2(E)} &\leqslant \|\mathsf{K}_E^{-1}\|_\infty\|\overline{F}-F^R_{h,E}\|_{L^2(E)}\\ &\leqslant \|\mathsf{K}_E^{-1}\|_\infty\|(\overline{F}^I-F_h)^R\|_{L^2(E)}\\ &\leqslant \|\mathsf{K}_E^{-1}\|_\infty\mathrm{Trace}(\mathsf{K}_E)^{1/2}\|\overline{F}^I-F_h\|_E\\ &\leqslant \|\mathsf{K}_E^{-1}\|_\infty\mathrm{Trace}(\mathsf{K}_E)^{1/2}(\|\overline{F}^I-F^I\|_E\\ &\quad+\|F^I-F_h\|_E).\end{aligned}$$

The first term in the right-hand side of the last inequality is bounded as follows by applying inequalities (8) and (22) for $i=1,\ldots,d$:

$$\begin{aligned}|||\overline{F}^I-F^I|||^2_E &\leqslant C^*|E|\sum_{e\in\partial E}|(\overline{F}^I-F^I)^e_E|^2\\ &\leqslant C^*|E|\sum_{e\in\partial E}\frac{1}{|e|}\int_e|n^e_E\cdot(\overline{F}-F(X))|^2\,\mathrm{d}S\\ &\leqslant C^*|E|\sum_{e\in\partial E}\\ &\quad\times\frac{1}{h_E^{d-1}}\left(\frac{1}{h_E}\|\overline{F}-F\|^2_{L^2(E)}+h_E|\overline{F}-F|^2_{H^1(E)}\right)\\ &\leqslant C^*k_E|E|h_E^{2-d}|F|^2_{H^1(E)}\leqslant C^*k_E\|\mathsf{K}_E\|^2_\infty h_E^2|p|^2_{H^2(E)}.\end{aligned}$$

Finally, we introduce the constants $C'=C^{*1/2}k_E^{1/2}\|\mathsf{K}_E\|_\infty\|\mathsf{K}_E^{-1}\|_\infty\mathrm{Trace}(\mathsf{K}_E)^{1/2}$ and $C''=\|\mathsf{K}_E^{-1}\|_\infty\mathrm{Trace}(\mathsf{K}_E)^{1/2}$, which are clearly independent of p and h_E. □

We are now ready to prove our main result.

Theorem 1. *Let $(p,\mathbf{F})$ be the solution of problem (1) under the assumption (2) and $p\in H^2(\Omega)$. Let, moreover, $(\mathbf{p}_h,\ \mathbf{F}_h)$ be the MFD solution given by (7a) and (7b), under the mesh regularity assumptions* (M1) *and* (M5) *and assumption* (L) *concerning the lifting operator. We have*

$$\|p-p^R_h\|_{L^2(\Omega)}\leqslant Ch^2(\|p\|_{H^2(\Omega)}+\|b\|_{H^1(\Omega)}).$$

Proof. Recall the notation $p^I=\{\bar{p}\}$ and $p_h=\{p_{h,E}\}$. By adding and subtracting the averaged Taylor's polynomial of order one and the term $\overline{\nabla p}\cdot(x-y)$ in the integral argument, and recalling the definition of $\bar{p}$, we get

$$\begin{aligned}\|p-p^R_h\|^2_{L^2(\Omega)} &= \sum_{E\in\mathscr{T}_h}\int_E|p(x)-p_{h,E}-\nabla_E p_h\cdot(x-x_E)|^2\,\mathrm{d}x\\ &\leqslant \mathscr{E}^{\mathrm{I}}+\mathscr{E}^{\mathrm{II}}+\mathscr{E}^{\mathrm{III}}+\mathscr{E}^{\mathrm{IV}},\end{aligned}$$

where

$$\mathscr{E}^{\mathrm{I}}=\sum_{E\in\mathscr{T}_h}\int_E\left|p(x)-\frac{1}{|E|}\int_E(p(y)+\nabla p(y)\cdot(x-y))\mathrm{d}y\right|^2\mathrm{d}x,$$

$$\mathscr{E}^{\mathrm{II}}=\sum_{E\in\mathscr{T}_h}\int_E|\bar{p}-p_{h,E}|^2\mathrm{d}x,$$

$$\mathscr{E}^{\mathrm{III}}=\sum_{E\in\mathscr{T}_h}\int_E\left|\frac{1}{|E|}\int_E(\nabla p(y)-\overline{\nabla p})\cdot(x-y)\mathrm{d}y\right|^2\mathrm{d}x,$$

$$\mathscr{E}^{\mathrm{IV}}=\sum_{E\in\mathscr{T}_h}\int_E\left|\frac{1}{|E|}\int_E(\overline{\nabla p}-\nabla_E p_h)\cdot(x-y)\mathrm{d}y\right|^2\mathrm{d}x.$$

The term $\mathscr{E}^{\mathrm{I}}$ is immediately bounded as follows

$$\mathscr{E}^{\mathrm{I}}\leqslant Ch^4|p|^2_{H^2(\Omega)}$$

by applying inequality (1) of Lemma 1. The term $\mathscr{E}^{\mathrm{II}}$ is bounded by noting that $\mathscr{E}^{\mathrm{II}}=|||p^I-p_h|||^2_{Q_h}$ and using (25). The term $\mathscr{E}^{\mathrm{III}}$ is bounded by using (20) with $u=\partial p/\partial x_i$ for $i=1,\ldots,d$:

$$\mathscr{E}^{\mathrm{III}}\leqslant C\sum_{E\in\mathscr{T}_h}\|\nabla p-\overline{\nabla p}\|^2_{L^2(E)}h_E^2\leqslant Ch_E^4|p|^2_{H^2(E)}.$$

Finally, the term $\mathscr{E}^{\mathrm{IV}}$ is bounded by using Lemma 4 and (23):

$$\begin{aligned}\mathscr{E}^{\mathrm{IV}} &\leqslant C\sum_{E\in\mathscr{T}_h}\|\overline{\nabla p}-\nabla_E p_h\|^2_{L^2(E)}h_E^2\\ &\leqslant 2C\sum_{E\in\mathscr{T}_h}\left[C'h_E^2|p|^2_{H^2(E)}+C''|||F^I-F_h|||^2_E\right]h_E^2\\ &\leqslant Ch^2(h^2|p|^2_{H^2(\Omega)}+|||F^I-F_h|||^2_{X_h})\leqslant Ch^4|p|^2_{H^2(\Omega)}.\end{aligned}$$ □

5. Numerical experiments

The super-convergence estimate (25) states that the MFD approximation of solution cell averages quadratically converges under very general conditions. On the other hand, the estimate of Theorem 4 confirms that a piecewise constant approximation of the exact solution must be at most first-order accurate in the L^2-norm. Further, Theorem

1 shows that a more accurate approximation of the scalar solution field is still possible by exploiting the super-convergence effect in the post-processing strategy discussed in Section 4. The aim of the following numerical experiments is to show that the post-processed solution field is more accurate than the basic MFD approximation when cell-averages superconverge.

We assess the performance of the post-processing method presented in Section 4 by comparing the two errors $|||p^I - p_h|||_{Q_h}$ and $\|p - p_h\|_{\mathrm{L}^2(\Omega)}$ for the discrete solution p_h with the error $\|p - p_h^R\|_{L^2(\Omega)}$ for the reconstructed field p_h^R. We also consider the rate of convergence of the numerical flux and the reconstructed gradient towards flux and gradient of the analytical solution. These approximation errors are measured by $|||F^I - F_h|||_{X_h}$ for the flux field and by using the two mesh-dependent norms

$$\mathscr{E}' = \frac{\left[\sum_E \int_E |\nabla p - \nabla_E p_h|^2 \,\mathrm{d}V\right]^{1/2}}{\|\nabla p\|_{L^2(\Omega)}}, \tag{26a}$$

$$\mathscr{E}'' = \frac{\left[\sum_E |E| \|\nabla p(X_E) - \nabla_E p_h|^2\right]^{1/2}}{\|\nabla p\|_{L^2(\Omega)}}, \tag{26b}$$

for the reconstructed gradient $\{\nabla_E p_h\}$. All numerical results are displayed as curves of relative errors in log–log plots. In all figures, the left plot corresponds to the error curves for the approximation of the scalar solution field, the right plot to the error curves for the approximation of flux and gradient.

We consider three test cases based on different mesh families. The meshes of the first test case are formed by convex elements (mainly hexagons), e.g. Fig. 1. The meshes of the second test case are formed by "L"-shaped (non-convex, non-matching) elements, e.g. Fig. 2. Finally, the meshes of the third test case are formed by randomly shaped quadrilaterals, e.g. Fig. 3. In this last test case, a different mesh resolution is imposed for $y < 1/2$ and $y > 1/2$ and non-matching nodes are present at the line interface $y = 1/2$. The mesh data structures are managed by a suitably modified version of P2MESH [4], a C++ public domain library designed for fast and efficient implementation of partial differential equation solvers. A common ingredient in the mesh construction for Test Cases 1 and 2 is the mapping $(\xi, \eta) \to (x, y)$ given by [11]

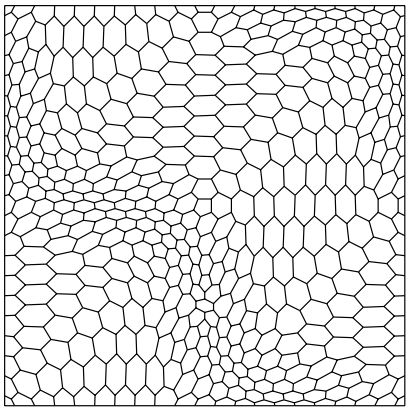

Fig. 1. Test Case 1. The polygonal mesh is formed by convex elements (mainly hexagons) and built by a dualization procedure starting from a Delaunay triangulation.

$$\begin{aligned} x &= \xi + (1/10)\sin(2\pi\xi)\sin(2\pi\eta), \\ y &= \eta + (1/10)\sin(2\pi\xi)\sin(2\pi\eta). \end{aligned} \tag{27}$$

Test Case 1 (*convex elements*). We solve the elliptic model problem (1) on the computational domain $\Omega = (0,1) \times (0,1)$ imposing the boundary data and forcing term so that

$$p(x, y) = \sin(2\pi x)\sin(2\pi y) + x^2 + y^2 + 1 \tag{28}$$

is the exact solution. Two choices of the diffusion tensor are considered: K equal to the identity matrix (constant diffusion tensor) and

$$\mathsf{K}(x, y) = \begin{bmatrix} (x+1)^2 + y^2 & -xy \\ -xy & (x+1)^2 \end{bmatrix}, \tag{29}$$

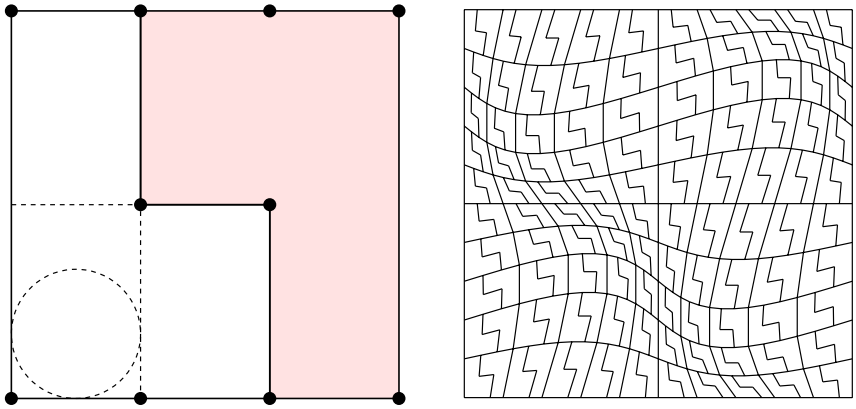

Fig. 2. Test Case 2. The left plot shows a detail about the construction of "L"-shaped non-convex elements: a square cell is split into two L-shaped elements; the bottom-left element is star-shaped, for instance, with respect to the dashed open ball depicted in the plot. The right plot shows the the polygonal mesh that is formed by "L"-shaped non-convex elements.

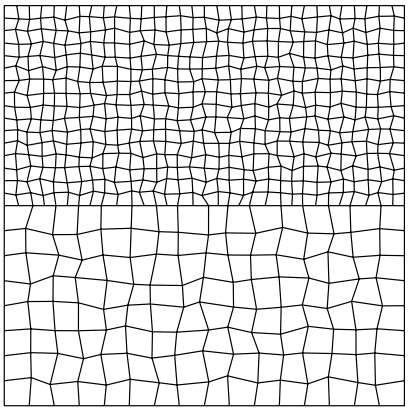

Fig. 3. Test Case 3. The non-matching polygonal mesh is formed by random-shaped quadrilaterals.

(non-constant diffusion tensor taken from Test Case 1 of Ref. [11]). In the latter case, a piecewise constant tensor K_E, as required by the MFD formulation, is provided by setting $\mathsf{K}_E = \mathsf{K}(\mathbf{x}_E)$ on each element E. As suggested in [11] one also may consider averaging the components of K.

The meshes considered in this test case, e.g. Fig. 1, are built as follows. We start from an $n \times n$ uniform mesh covering Ω, remap the node positions by using (27), build a Delaunay triangulation of these nodes by means of the mesh generator TRIANGLE [29,30] and finally apply the following dualization procedure. For any node, we build the corresponding dual element by connecting the barycenters of adjacent Delaunay triangular cells. The construction of boundary dual elements must be completed by connecting the barycenter of the triangular cells adjacent to Γ to the boundary edge midpoints and these latters to the corresponding boundary node. The first mesh is obtained by setting $n = 20$, and the refined meshes are generated by doubling this parameter and repeating the construction procedure used to build the base mesh.

The numerical results are shown in Figs. 4 and 5. As predicted by Theorem 1, the post-processed solution of Definition 3 is quadratically convergent in the L^2-norm. The piecewise constant approximation to the scalar solution is superconvergent in the discrete $|||\cdot|||_{Q_h}$-norm, but it is only first-order accurate in the L^2-norm. By comparing the left plots of Figs. 4 and 5, we also note that the errors in the case of constant diffusion are a factor of two-three smaller than those of non-constant diffusion (29), but the convergence behavior is similar. The right plots of Figs. 4 and 5 show the expected linear convergence of the flux approximation in $|||\cdot|||_{X_h}$ and for the reconstructed gradients.

In the case of non-constant diffusion, we also investigated how the performance of the reconstruction algorithm depends on the scalar product of X_h. Recall that this latter depends on the correction term (14) through the parameter u. The plots in Fig. 6 represent relative error curves of the mimetic approximation, the reconstructed solution, and the reconstructed gradient in function of u. These experimental results are obtained on the base mesh by varying the parameter u in the range $[10^{-8},10^{4}]$. Note the superposition of the error curves of the post-processed solution in the L^2-norm and of the piecewise constant solution in the discrete norm for the full parameter range. An optimal value of u is clearly visible where the mimetic scheme and the reconstruction algorithm attain the best performance, i.e. minimum approximation error. Nonetheless, the choice of u is not critical as a wide set of parameter values gives nearly optimal results. This fact was already point it out in [11], where a similar experiment was presented to study how the mimetic scheme performance depends on the scalar product of X_h. We finally remark the "plateau" in all these curves for the smallest values of u, e.g. $u \leqslant 10^{-4}$: the scheme performance is not degenerating as the correction term becomes small and, consequently, the scalar product matrix tends to a non positive-definite matrix.

The errors on flux and reconstructed gradients are shown in the right plot of Fig. 6. The errors are of the same order of magnitude in a wide range of values of u. Notice that the gradient error at barycenters (dot-dashed line) is

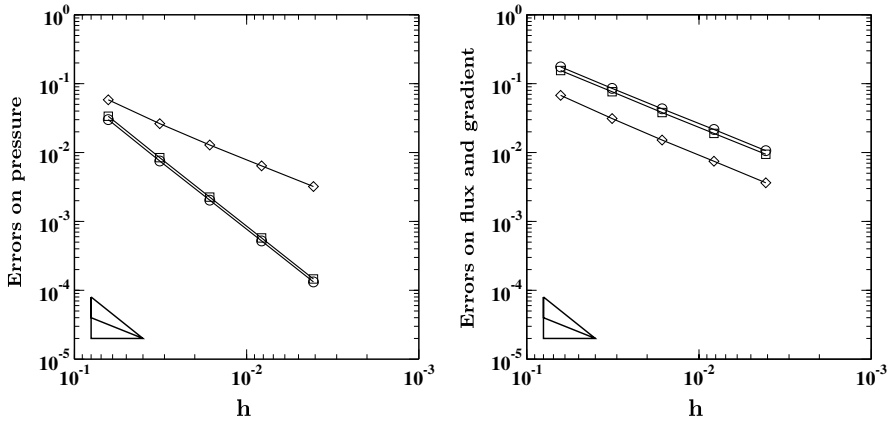

Fig. 4. Test Case 1: convex polygonal meshes and constant diffusion tensor K. Left plot: relative error curves for pressure using $|||p^I - p_h|||_{Q_h}$ (circles), $\|p - p_h^R\|_{L^2(\Omega)}$ (squares), and $\|p - p_h\|_{L^2(\Omega)}$ (diamond). Right plot: relative error curves for flux and gradients using $|||F^I - F_h|||_{X_h}$ (circles), $\mathscr{E}'$, see (26a), (squares), and $\mathscr{E}''$, see (26b), (diamonds). For reference's sake, first- and second-order slopes are reported near the bottom-left corner.

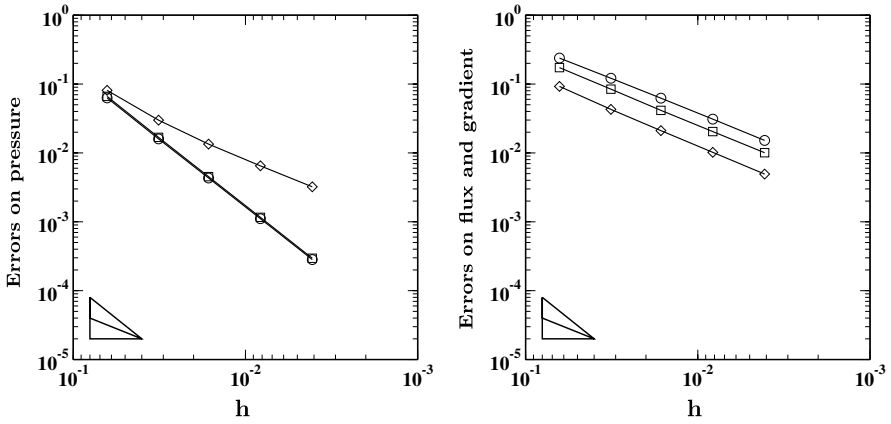

Fig. 5. Test Case 1: convex polygonal meshes and non-constant diffusion tensor K. Left plot: relative error curves for pressure using $|||p^I - p_h|||_{Q_h}$ (circles), $\|p - p_h^R\|_{L^2(\Omega)}$ (squares), and $\|p - p_h\|_{L^2(\Omega)}$ (diamond). Right plot: relative error curves for flux and gradients using $|||F^I - F_h|||_{X_h}$ (circles), $\mathscr{E}'$, see (26a), (squares), and $\mathscr{E}''$, see (26b), (diamonds). For reference's sake, first- and second-order slopes are reported near the bottom-left corner.

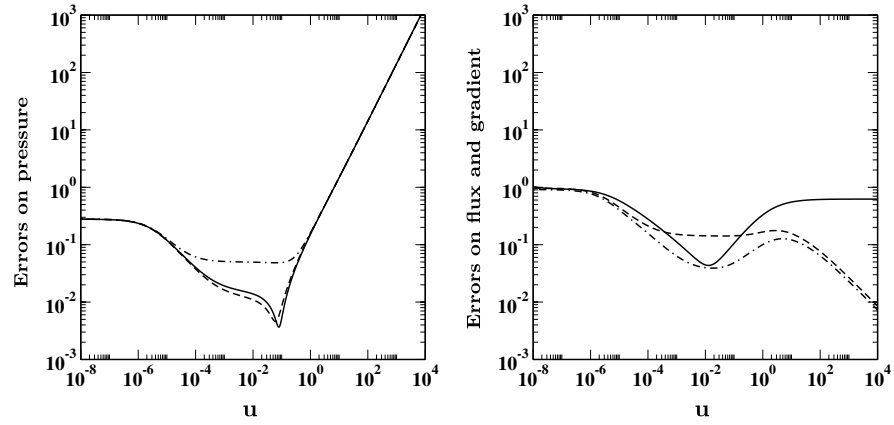

Fig. 6. Test Case 1: convex polygonal meshes and non-constant diffusion tensor K. Left plot: relative error curves for pressure versus u using $|||p^I - p_h|||_{Q_h}$ (continuous line), $\|p - p_h^R\|_{L^2(\Omega)}$ (dashed line), and $\|p - p_h\|_{L^2(\Omega)}$ (dot-dashed line). Right plot: relative error curves for flux and gradients using $|||F^I - F_h|||_{X_h}$ (continuous line), $\mathscr{E}'$, see (26a), (dashed line), and $\mathscr{E}''$, see (26b), (dot-dashed line).

smaller than the flux error in the X_h-norm (continuous line).

Test Case 2 (*non-convex elements*). We repeat the same calculations of Test Case 1 by solving (28) with diffusion tensor given by a scalar multiple of the identity matrix and by (29) on a different family of meshes. The meshes considered in this test case are formed by non-convex elements given by sub-dividing each square of the $n \times n$ uniform mesh into two "L"-shaped sub-elements formed by seven nodes and seven edges. This splitting introduces four new nodes on the boundary and two new nodes in the interior of the original square element with non-matching nodes inside the horizontal edges. This procedure is illustrated in Fig. 2 (left). Finally, all the nodes are repositioned inside Ω according to the coordinate mapping (27). The starting mesh is obtained by setting $n = 10$ and is shown in the right plot of Fig. 2. The successive refinements are obtained by doubling the parameter n.

With this test case we aim to investigate the influence of the shape of the elements on the reconstruction procedure. As shown by Figs. 7 and 8, the post-processed numerical solution is still converging quadratically to the exact solution. The relative errors are only a factor of two-three greater than the errors shown in the corresponding plots of Test Case 1. Thus, the quality of the approximation provided by the MFD scheme on the "L"-shaped meshes and convex meshes is comparable.

Test Case 3 (*non-matching random-shaped quadrilaterals*). We test the reconstruction algorithm on a problem whose solution is not in $H^2(\Omega)$. We solve the boundary value problem (1) on the computational domain $\Omega = (0,1) \times (0,1)$ with

$$\mathsf{K}(x,y) = \begin{cases} K_1 I & \text{for } y < 1/2, \\ K_2 I & \text{for } y \geqslant 1/2, \end{cases}$$

where K_1 and K_2 are two positive constants and $\mathbf{I}$ is the identity matrix. The boundary data and forcing term are set according to

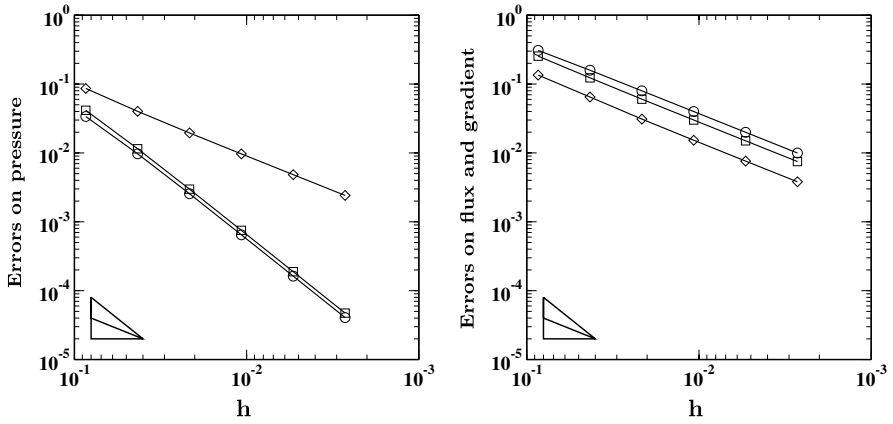

Fig. 7. Test Case 2: non-convex polygonal meshes and constant diffusion tensor K. Left plot: relative error curves for pressure using $|||p^I - p_h|||_{Q_h}$ (circles), $\|p - p_h^R\|_{L^2(\Omega)}$ (squares), and $\|p - p_h\|_{L^2(\Omega)}$ (diamond). Right plot: relative error curves for flux and gradients using $|||F^I - F_h|||_{X_h}$ (circles), $\mathscr{E}'$, see (26a), (squares), and $\mathscr{E}''$, see (26b), (diamonds). For reference's sake, first- and second-order slopes are reported near the bottom-left corner.

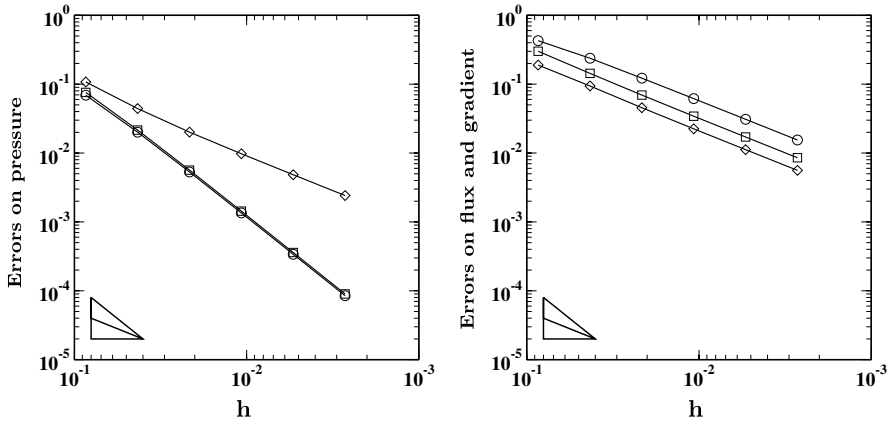

Fig. 8. Test Case 2: non-convex polygonal meshes and non-constant diffusion tensor K. Left plot: relative error curves for pressure using $|||p^I - p_h|||_{Q_h}$ (circles), $\|p - p_h^R\|_{L^2(\Omega)}$ (squares), and $\|p - p_h\|_{L^2(\Omega)}$ (diamond). Right plot: relative error curves for flux and gradients using $|||F^I - F_h|||_{X_h}$ (circles), $\mathscr{E}'$, see (26a), (squares), and $\mathscr{E}''$, see (26b), (diamonds). For reference's sake, first- and second-order slopes are reported near the bottom-left corner.

$$p(x,y) = \begin{cases} a + bx + cy^m & \text{for } y < 1/2, \\ a + c\frac{K_2 - K_1}{2^m K_2} + bx + c\frac{K_1}{K_2} y^m & \text{for } y \geqslant 1/2. \end{cases}$$

For $m = 1$ the exact solution is linear above and below $y = 1/2$. Note also that the solution and the co-normal

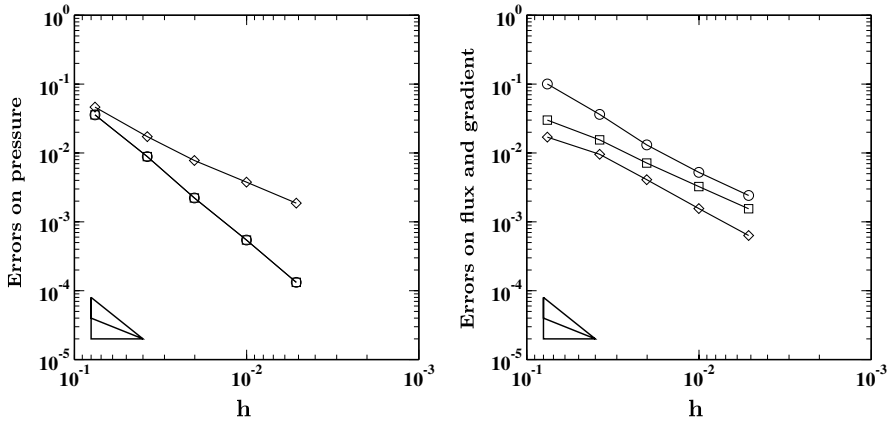

Fig. 9. Test Case 3: non-matching meshes of random-shaped quadrilaterals and discontinuous diffusion tensor K. Left plot: relative error curves for pressure using $|||p^I - p_h|||_{Q_h}$ (circles), $\|p - p_h^R\|_{L^2(\Omega)}$ (squares), and $\|p - p_h\|_{L^2(\Omega)}$ (diamond). Right plot: relative error curves for flux and gradients using $|||F^I - F_h|||_{X_h}$ (circles), $\mathscr{E}'$, see (26a), (squares), and $\mathscr{E}''$, see (26b), (diamonds). For reference's sake, first- and second-order slopes are reported near the bottom-left corner.

derivative are continuous at $y = 1/2$, but the normal derivative is not. In accordance with the similar test case proposed in [11], we take $a = b = c = 1$, $m = 3$, $K_1 = 10$ and $K_2 = 1$. We consider a sequence of non-matching meshes of randomly shaped quadrilaterals, cf. Fig. 3. These are generated as follows. We consider two uniform meshes of square-shaped cells with different resolution below and above the interface line $y = 1/2$. Each vertex that is strictly below or above $y = 1/2$ is randomly moved inside a square that is centered at the original position of the vertex and having a side long equal to 0.8 times the smallest edge of the uniform mesh. In order to maintain fixed the interface line, only the abscissa of vertexes lying at $y = 1/2$ is allowed to move. Let n be the parameter controlling the mesh resolution. The uniform mesh below $y = 1/2$ is formed by $2n \times n$ squares, while the mesh above $y = 1/2$ by $2n \times 2n$ squares. Notice that the polygons that are immediately below the line $y = 1/2$ are (degenerate) pentagons with two parallel consecutive edges.

The numerical results displayed in Fig. 9 show that also in this case convergence is optimal. Note that the error curves for the reconstructed solution p_h^R in the L^2-norm and the piecewise constant solution p_h in the $|||\cdot|||_{\mathcal{Q}_h}$-norm nearly coincide. The reconstructed gradient converges linearly, *cf.* the plot on the right of Fig. 9.

6. Conclusions

The MFD method of Refs. [8,11] is a low order scheme for elliptic boundary value problems that provides a piecewise constant approximation of the scalar solution. In this paper, we developed a post-processing technique for computing a piecewise linear approximation of the solution field. Starting from the mimetic flux solution, we construct a constant elemental gradient which is then used to define a linear approximation to the scalar solution field within each element. We proved that the post-processed solution is second-order accurate in the L^2-norm under very general assumptions. Numerical experiments using meshes with convex, non-convex and non-matching elements and constant and non-constant diffusion tensors confirmed the optimal behavior of the post-processing technique.

Acknowledgement

We would like to thank Prof. Franco Brezzi for useful discussions and suggestions.

Appendix. Proof of Lemma 1

We start by proving the statement for a function $u \in \mathrm{C}^\infty(\Omega)$. Let $\widetilde{\Omega}$ be the convex hull of Ω and $\tilde{u}$ be an extension of u to $\widetilde{\Omega}$ whose norm is bounded by that of u. Such an extension exists as Ω is bounded and has Lipschitz continuous boundary, see e.g. [1]. Moreover, let $\widetilde{E}$ be the convex hull of the generic element E.

The first-order Taylor's expansion of $u(\mathbf{x})$ around $\mathbf{y} \in E$ reads

$$u(x) = u(y) + \nabla u(y) \cdot (x - y) + \mathsf{R}(x, y; \tilde{u}),$$

where the last term is the Taylor's remainder

$$\mathsf{R}(x, y; \tilde{u}) = \sum_{i,j=1}^{d} c_{ij}(x_i - y_i)(x_j - y_j) \int_0^1 s\partial_{ij}^2 \tilde{u}(x + s(y - x))\mathrm{d}s$$

where $\partial_{ij}^2 \tilde{u}$ represents the second derivative of $\tilde{u}$ with respect to the ith and jth arguments, and $c_{ij} = 1/2$ for $i = j$, $c_{ij} = 1$ for $i \neq j$. As $|x_i - y_i| \leqslant h_E$ for any $i = 1, \ldots, d$, we readily obtain:

$$\begin{aligned}
&\int_{y\in E} |\mathsf{R}(x, y; \tilde{u})|\,\mathrm{d}y \\
&\quad \leqslant h_E^2 \sum_{i,j=1}^{d} \int_{y\in E} \left| \int_0^1 s\partial_{ij}^2 \tilde{u}(x + s(y - x))\mathrm{d}s \right| \mathrm{d}y \\
&\quad \leqslant h_E^2 \int_0^1 s \left[\sum_{i,j=1}^{d} \int_{y\in E} \left| \partial_{ij}^2 \tilde{u}(x + s(y - x)) \right| \mathrm{d}y \right] \mathrm{d}s.
\end{aligned}$$

By using the affine mapping $\boldsymbol{\xi} = \mathbf{x} + s(\mathbf{y} - \mathbf{x})$ we reformulate the integral on $\mathbf{y} \in E$ into an integral on $\boldsymbol{\xi} \in \widehat{E}(s)$ where $\widehat{E}(s) = \{\boldsymbol{\xi} : \boldsymbol{\xi} = x + s(y - x) \text{ for } y \in E\}$:

$$\begin{aligned}
&\int_{y\in E} |\mathsf{R}(x, y; \tilde{u})|\,\mathrm{d}y \\
&\quad \leqslant h_E^2 \int_0^1 s^{1-d} \left[\sum_{i,j=1}^{d} \int_{\xi\in \widehat{E}(s)} |\partial_{ij}^2 \tilde{u}(\boldsymbol{\xi})| \mathrm{d}\boldsymbol{\xi} \right] \mathrm{d}s \\
&\quad \leqslant h_E^2 \int_0^1 s^{1-d} |\widehat{E}(s)|^{\frac{1}{2}} \left[\sum_{i,j=1}^{d} \int_{\xi\in \widehat{E}(s)} |\partial_{ij}^2 \tilde{u}(\boldsymbol{\xi})|^2 d\boldsymbol{\xi} \right]^{\frac{1}{2}} \mathrm{d}s \\
&\quad = h_E^2 \int_0^1 s^{1-\frac{d}{2}} |\widetilde{E}|^{\frac{1}{2}} |\tilde{u}|_{H^2(\widehat{E}(s))} \mathrm{d}s,
\end{aligned}$$

as $|\widehat{E}(s)| \leqslant s^d |\widetilde{E}|$. Further, as $\widehat{E}(s) \subseteq |\widetilde{E}|$ we obtain the final estimate

$$\int_{y\in E} |\mathsf{R}(x, y; \tilde{u})|\,\mathrm{d}y \leqslant \frac{2}{4 - d} h_E^2 |\widetilde{E}|^{\frac{1}{2}} |\tilde{u}|_{H^2(\widetilde{E})}.$$

A density argument extends this result to all functions in $H^2(\widetilde{E})$.

We now prove inequality (21). For every $u \in H^2(\Omega)$ we have

$$\begin{aligned}
&\sum_{E\in\mathscr{T}_h} \int_{x\in E} \left| u(x) - \frac{1}{|E|} \int_{y\in E} (u(y) + \nabla u(y) \cdot (x - y))\,\mathrm{d}y \right|^2 \mathrm{d}x \\
&\quad \leqslant \sum_{E\in\mathscr{T}_h} \frac{1}{|E|^2} \int_{x\in E} \left[\int_{y\in E} |\mathsf{R}(x, y; \tilde{u})|\,\mathrm{d}y \right]^2 \mathrm{d}x \\
&\quad \leqslant \sum_{E\in\mathscr{T}_h} \frac{|\widetilde{E}|}{|E|} \frac{4h_E^4}{(2 - d)^2} |\tilde{u}|_{H^2(\widetilde{E})}^2 \leqslant Ch^4 \sum_{E\in\mathscr{T}_h} |\tilde{u}|_{H^2(\widetilde{E})}^2 \\
&\quad \leqslant Ch^4 |\tilde{u}|_{H^2(\widetilde{\Omega})}^2 \leqslant Ch^4 |u|_{H^2(\Omega)}^2,
\end{aligned}$$

as from the shape regularity assumptions it follows that $|\widetilde{E}| \leqslant C|E|$ and that $\widetilde{E}$ is contained in the union of a finite number of elements.

References

[1] R.A. Adams, J.J.F. Fournier, Sobolev spaces, Pure and Applied Mathematics, vol. 140, Academic Press, New York-London, 2003.

[2] D. Arnold, P. Bochev, R. Lehoucq, R. Nicolaides, M. Shashkov (Eds.), Compatible discretizations, Proceedings of IMA hot topics workshop on compatible discretizations, IMA Volume 142, Springer-Verlag, 2006.

[3] M. Berndt, K. Lipnikov, D. Moulton, M. Shashkov, Convergence of mimetic finite difference discretizations of the diffusion equation, East-West J. Numer. Math. 9 (4) (2001) 265–284.

[4] E. Bertolazzi, G. Manzini, Algorithm 817 P2MESH: generic object-oriented interface between 2-D unstructured meshes and FEM/FVM-based PDE solvers, ACM Trans. Math. Softw. 28 (1) (2002) 101–132.

[5] E. Bertolazzi, G. Manzini, A cell-centered second-order accurate finite volume method for convection–diffusion problems on unstructured meshes, Math. Models Methods Appl. Sci. 8 (2004) 1235–1260.

[6] E. Bertolazzi, G. Manzini, A second-order maximum principle preserving finite volume method for steady convection–diffusion problems, SIAM J. Numer. Anal. 43 (5) (2006) 2172–2199.

[7] E. Bertolazzi, G. Manzini, On vertex reconstructions for cell-centered finite volume approximations of 2-D anisotropic diffusion problems, Math. Models Methods Appl. Sci. 17 (1) (2007) 1–32.

[8] F. Brezzi, K. Lipnikov, M. Shashkov, Convergence of the mimetic finite difference method for diffusion problems on polyhedral meshes, SIAM J. Numer. Anal. 43 (5) (2005) 1872–1896.

[9] F. Brezzi, K. Lipnikov, M. Shashkov, Convergence of mimetic finite difference method for diffusion problems on polyhedral meshes with curved faces, Math. Models Methods Appl. Sci. 16 (2) (2006) 275–297.

[10] F. Brezzi, K. Lipnikov, M. Shashkov, V. Simoncini, A new discretization methodology for diffusion problems on generalized polyhedral meshes, Comput. Methods Appl. Mech. Engrg. 196 (2007) 3682–3692.

[11] F. Brezzi, K. Lipnikov, V. Simoncini, A family of mimetic finite difference methods on polygonal and polyhedral meshes, Math. Models Methods Appl. Sci. 15 (10) (2005) 1533–1551.

[12] J.C. Campbell, M.J. Shashkov, A tensor artificial viscosity using a mimetic finite difference algorithm, J. Comput. Phys. 172 (2) (2001) 739–765.

[13] K. Domelevo, P. Omnes, A finite volume method for the Laplace equation on almost arbitrary two-dimensional grids, Math. Model. Numer. Anal. 39 (6) (2005) 1203–1249.

[14] J. Hyman, J. Morel, M. Shashkov, S. Steinberg, Mimetic finite difference methods for diffusion equations, Comput. Geosci. 6 (3–4) (2002) 333–352.

[15] J. Hyman, M. Shashkov, Mimetic discretisations of Maxwell's equations and the equations of magnetic diffusion, Prog. Electromagn. Res. 32 (2001) 89–121.

[16] J. Hyman, M. Shashkov, S. Steinberg, The numerical solution of diffusion problems in strongly heterogeneous non-isotropic materials, J. Comput. Phys. 132 (1) (1997) 130–148.

[17] J.M. Hyman, M. Shashkov, Adjoint operators for the natural discretizations of the divergence, gradient and curl on logically rectangular grids, Appl. Numer. Math. 25 (4) (1997) 413–442.

[18] J.M. Hyman, M. Shashkov, Approximation of boundary conditions for mimetic finite-difference methods, Comput. Math. Appl. 36 (5) (1998) 79–99.

[19] J.M. Hyman, M. Shashkov, The orthogonal decomposition theorems for mimetic finite difference methods, SIAM J. Numer. Anal. 36 (3) (1999) 788–818.

[20] J.M. Hyman, S. Steinberg, The convergence of mimetic discretization for rough grids, Comput. Math. Appl. 47 (10–11) (2004) 1565–1610.

[21] Y. Kuznetsov, K. Lipnikov, M. Shashkov, The mimetic finite difference method on polygonal meshes for diffusion-type problems, Comput. Geosci. 8 (4) (2004) 301–324, 2005.

[22] K. Lipnikov, J. Morel, M. Shashkov, Mimetic finite difference methods for diffusion equations on non-orthogonal non-conformal meshes, J. Comput. Phys. 199 (2004) 589–597.

[23] K. Lipnikov, M. Shashkov, D. Svyatskiy, The mimetic finite difference discretization of diffusion problem on unstructured polyhedral meshes, J. Comput. Phys. 211 (2) (2006) 473–491.

[24] R. Liska, M. Shashkov, V. Ganzha, Analysis and optimization of inner products for mimetic finite difference methods on a triangular grid, Math. Comput. Simulat. 67 (1–2) (2004) 55–66.

[25] J.E. Morel, M.L. Hall, M.J. Shashkov, A local support-operators diffusion discretization scheme for hexahedral meshes, J. Comput. Phys. 170 (1) (2001) 338–372.

[26] M. Shashkov, Conservative finite-difference methods on general grids, Symbolic and Numeric Computation Series, CRC Press, Boca Raton, FL, 1996, with 1 IBM-PC floppy disk (3.5 inch; HD).

[27] M. Shashkov, S. Steinberg, Support-operator finite-difference algorithms for general elliptic problems, J. Comput. Phys. 118 (1) (1995) 131–151.

[28] M. Shashkov, S. Steinberg, Solving diffusion equations with rough coefficients in rough grids, J. Comput. Phys. 129 (2) (1996) 383–405.

[29] J.R. Shewchuk, Triangle: engineering a 2D quality mesh generator and Delaunay triangulator, in: FCRC'96/WACG'96: Selected papers from the Workshop on Applied Computational Geormetry, Towards Geometric Engineering, Springer-Verlag, London, UK, 1996.

[30] J.R. Shewchuk, Delaunay refinement algorithms for triangular mesh generation, Comput. Geom.: Theory Appl. 22 (1–3) (2002) 21–74.